

Applications of Trench and Trajectory Friction Pendulum Systems to Seismic Mitigation of Structures

C. S. Tsai¹, Po-Ching Lu², Wen-Shin Chen³, Yung-Chang Lin²

¹ Professor, Department of Civil Engineering, Feng Chia University, Taichung, Chinese Taiwan.

² Ph. D. candidate, Graduate Institute of Civil and Hydraulic Engineering, Feng Chia University, Taichung, Chinese Taiwan.

³ Ph. D., Graduate Institute of Civil and Hydraulic Engineering, Feng Chia University, Taichung, Chinese Taiwan. Email: cstsai@fcu.edu.tw

ABSTRACT:

To promote earthquake resistance capability of structures and simplify the manufacturing processes of an isolator, two new base isolation systems called the trench friction pendulum system (TFPS) and the trajectory friction pendulum system (TFPS) are proposed and investigated to address their mechanical characteristics and performance in seismic mitigation through a series of shaking table tests in this study. The TFPS isolators can provide different natural periods, displacement capacity and damping effect in any two independent directions. Results from the shaking table tests of a scaled three-story structure isolated with TFPS isolators illustrate that the proposed TFPS isolators can isolate most seismic energy trying to impart to the structure and provide good protection for structures from earthquake damage. In addition, comparisons between experimental results and numerical analyses by the derived mathematical formulation demonstrate that the proposed mathematical model can predict the response of a structure isolated with TFPS isolators with high accuracy.

KEYWORDS: Earthquake Engineering, Base Isolation, Passive Control, Friction Pendulum System, Base Isolator

1. INTRODUCTION

The application of the base isolation technology to promoting earthquake resistance capability of structures has a long history and has been accepted as a feasible and attractive way for structures in seismic mitigation. In this paper, an innovative base isolator called the trench friction pendulum system (TFPS), as shown in Figure 1, has been proposed to update the capability of structures in seismic mitigation. The proposed TFPS isolator consists of the upper and lower trench concave surfaces which orthogonally cross to each other and an articulated slider, as shown as Figures 1. The slider possesses a special articulated mechanism and is located between the upper and lower trench concave surfaces to accommodate any rotations in the isolator induced by various loadings and maintain the stability of isolated structures during earthquakes. Lengthening the individual natural periods of a structure in two orthogonal directions can be designed by different radii in the upper and lower trench concave surfaces. The contents of this study are mainly grouped into two parts: (i) the mathematical formulation for the TFPS isolator; and (ii) shaking table tests and numerical simulation of a steel structure isolated with TFPS isolators. The results from a series of shaking table tests of a steel structure with TFPS isolators illustrate that the TFPS isolator is an effective tool to promoting the seismic resistance capability of structures. Moreover, numerical simulations using the proposed formulations included in the NSAT computer program [1] express that the behavior of a steel structure isolated with TFPS isolators can be well simulated by the proposed formulations under seismic loadings.

2. MATHEMATICAL FORMULATIONS FOR TFPS ISOLATOR

The mechanical behavior of the TFPS isolator is similar to MFPS isolator when subjected to earthquakes in a single direction [2-5, 6, 7]. The only difference is that the force in the orthogonal direction would influence each other in a way of frictional forces as two-directional ground motions simultaneously act on the TFPS isolator. Figure 2 is the top view of the lower trench concave surface with the slider in the X-direction. Therefore, on the basis of the mechanical behavior of the TFPS isolator which is similar to the MFPS isolator

[2-5, 6, 7] and the concept of the force increment, the horizontal force increment of the lower trench concave surface can be written as:

$$dF_x = \frac{W}{R_x} du_x + |d\mu_x| W \operatorname{sgn}\left(\frac{du_x}{dt}\right) + |\mu_{sx}| dF_y \operatorname{sgn}(dF_y) \operatorname{sgn}\left(\frac{du_x}{dt}\right) \quad (1)$$

where W is the vertical loading resulting from the superstructure, which includes the gravity and earthquake induced loadings; R_x indicates the radius of lower trench concave surface in the X-direction; $d\mu_x$ is the friction coefficient increment at the bottom of lower trench concave surface, which is a function of velocities; du_x indicates the horizontal relative displacement increment in the X direction between the slider and the lower trench concave surface; μ_{sx} is the friction coefficient at the side wall of the lower trench concave surface; dF_y indicates the horizontal force increment of the upper trench concave surface in the Y-direction.

However, as a result of $\operatorname{sgn}\left(\frac{du_x}{dt}\right) = \operatorname{sgn}(du_x)$, equation (1) can be rewritten as:

$$dF_x = \frac{W}{R_x} du_x + |d\mu_x| W \operatorname{sgn}(du_x) + |\mu_{sx}| dF_y \operatorname{sgn}(dF_y) \operatorname{sgn}(du_x) \quad (2)$$

Furthermore, Figure 3 is the top view of the upper trench concave surface with the slider in the Y direction. Following the same concept, the horizontal force increment in the Y-direction can be given as

$$dF_y = \frac{W}{R_y} du_y + |d\mu_y| W \operatorname{sgn}(du_y) + |\mu_{sy}| dF_x \operatorname{sgn}(dF_x) \operatorname{sgn}(du_y) \quad (3)$$

where R_y indicates the radius of the upper trench concave surface in the Y-direction; $d\mu_y$ is the friction coefficient increment at the bottom of the upper trench concave surface, which is a function of velocity; du_y indicates the relative horizontal displacement increment between the slider and the upper trench concave surface in the Y-direction; μ_{sy} is the friction coefficient at the side wall of the upper trench concave surface; dF_x indicates the horizontal force increment of the lower trench concave surface, which is in the X-direction.

Backsubstituting equation (3) into equation (2), the horizontal force increment of lower trench concave surface, dF_x , can be given by

$$dF_x = \frac{1}{[1 - |\mu_{sx}| |\mu_{sy}| dF_x \operatorname{sgn}(dF_x) \operatorname{sgn}(dF_y) \operatorname{sgn}(du_x) \operatorname{sgn}(du_y)]} \left[\frac{W}{R_x} du_x + |\mu_{sx}| \frac{W}{R_y} du_y \operatorname{sgn}(dF_y) \operatorname{sgn}(du_x) \right] + \frac{1}{[1 - |\mu_{sx}| |\mu_{sy}| dF_x \operatorname{sgn}(dF_x) \operatorname{sgn}(dF_y) \operatorname{sgn}(du_x) \operatorname{sgn}(du_y)]} \left[|d\mu_x| W \operatorname{sgn}(du_x) + |\mu_{sx}| |d\mu_y| W \operatorname{sgn}(du_y) \operatorname{sgn}(dF_y) \operatorname{sgn}(du_x) \right] \quad (4)$$

If we set $a = [1 - |\mu_{sx}| |\mu_{sy}| dF_x \operatorname{sgn}(dF_x) \operatorname{sgn}(dF_y) \operatorname{sgn}(du_x) \operatorname{sgn}(du_y)]$, the formulation in equation (4) can be rewritten as:

$$dF_x = \frac{1}{a} \left[\frac{W}{R_x} du_x + |\mu_{sx}| \frac{W}{R_y} du_y \operatorname{sgn}(dF_y) \operatorname{sgn}(du_x) \right] + \frac{1}{a} \left[|d\mu_x| W \operatorname{sgn}(du_x) + |\mu_{sx}| |d\mu_y| W \operatorname{sgn}(du_y) \operatorname{sgn}(dF_y) \operatorname{sgn}(du_x) \right] \quad (5)$$

Similarly, back substituting equation (2) into equation (3), the horizontal force increment of the upper trench concave surface can be expressed as

$$dF_y = \frac{1}{a} \left[\frac{W}{R_y} du_y + |\mu_{sy}| \frac{W}{R_x} du_x \operatorname{sgn}(dF_x) \operatorname{sgn}(du_y) \right] + \frac{1}{a} \left[|d\mu_y| W \operatorname{sgn}(du_y) + |\mu_{sy}| |d\mu_x| W \operatorname{sgn}(du_x) \operatorname{sgn}(dF_x) \operatorname{sgn}(du_y) \right] \quad (6)$$

Rearrangement of equation (5) and equation (6), it can be obtained as:

$$\begin{aligned} \begin{Bmatrix} dF_x \\ dF_y \end{Bmatrix} &= \frac{1}{a} \begin{bmatrix} \frac{W}{R_x} & |\mu_{sx}| \frac{W}{R_y} \operatorname{sgn}(dF_y) \operatorname{sgn}(du_x) \\ |\mu_{sy}| \frac{W}{R_x} \operatorname{sgn}(dF_x) \operatorname{sgn}(du_y) & \frac{W}{R_y} \end{bmatrix} \begin{Bmatrix} du_x \\ du_y \end{Bmatrix} \\ &+ \frac{1}{a} \begin{Bmatrix} |d\mu_x| W \operatorname{sgn}(du_x) + |\mu_{sx}| |d\mu_y| W \operatorname{sgn}(du_y) \operatorname{sgn}(dF_y) \operatorname{sgn}(du_x) \\ |d\mu_y| W \operatorname{sgn}(du_y) + |\mu_{sy}| |d\mu_x| W \operatorname{sgn}(du_x) \operatorname{sgn}(dF_x) \operatorname{sgn}(du_y) \end{Bmatrix} \end{aligned} \quad (7)$$

In a matrix form, equation (7) can be rewritten as

$$d\mathbf{F} = \mathbf{K}d\mathbf{u} + d\mathbf{F}_f \quad (8)$$

Moreover, the natural frequencies of the TFPS isolator can be obtained by solving the equation, $\det[\mathbf{K} - \omega^2\mathbf{M}] = 0$ and it can be given by .

$$\omega^2 = \frac{W}{aR_x} + \frac{W}{aR_y} \pm \sqrt{\left(\frac{W}{aR_x} + \frac{W}{aR_y}\right)^2 - \frac{4W^2}{a^2R_xR_y}(1 - |\mu_{sx}||\mu_{sy}|)} \quad (9)$$

For a special case, $R_x = R_y = R$, the natural frequency of the TFPS isolator can be given as:

$$\omega^2 = \frac{g}{aR} \pm \frac{g}{aR} \sqrt{|\mu_{sx}||\mu_{sy}|} \quad (10)$$

3. SHAKING TABLE TEST AND SIMULATION FOR STRUCTURE ISOLATED WITH TRENCH FRICTION PENDULUM SYSTEM

An insight into the behavior of the TFPS in seismic mitigation would be helpful for engineers to realize and assess the feasibility on the actual practice. In order to examine the efficiency of a structure isolated with the TFPS isolator under seismic loadings, a series of shaking table tests were performed in the Department of Civil Engineering, Feng Chia University, Taichung, Chinese Taiwan. As shown in Figure 4, the tested building is a three story scaled-steel structure with a length of 1.1m in each horizontal direction, and 0.9m in height for each story. In addition, the trusses were installed in the diagonal direction. Each floor was equipped with a mass of 400kg, and the total mass of the structure is about 2.16tons. The natural frequency of the fixed base structure is about 10.6Hz. An electric power earthquake simulator was utilized to simulate the ground motions. In this study, the El Centro, Kobe and Chi-Chi (TCU084 station) earthquakes were adopted for the seismic input. As shown in Figure 6, four TFPS isolators, one for each column, had been installed at the bottom of columns.

Figures 5 and 6 respectively show the comparisons of roof acceleration responses of the structure with and without TFPS isolators under the El Centro and Chi-Chi (TCU 084 Station) earthquakes of 0.63g in PGA. Among these earthquakes, the Chi-Chi (TCU 084 Station) earthquake belongs to the near-fault ground motions. It was found from these figures that most responses induced by earthquakes with various levels of PGAs have been significantly reduced by the TFPS isolators. In addition, Table 1 shows that the proposed isolator provides an excellent efficiency in seismic mitigation. Figures 7 and 8 show the isolator displacement. Obviously, it is found that the TFPS isolator provides good restoring capability under various earthquakes at different levels of PGAs. Figures 9 and 10 display the hysteresis loops of the TFPS isolators during earthquakes and it illustrates that the TFPS isolator can provide significant damping in reducing the bearing displacement during earthquakes.

In order to simulate the behavior of a structure with TFPS isolators subjected to seismic loadings, the mathematical formulations derived in this paper were implemented in the NSAT computer program [20] and were used to simulate the response of the tested building with proposed isolators under various ground motions. Figures 11 and 12 show the comparison of the roof acceleration between experimental and numerical results under the El Centro, Kobe and Chi-Chi earthquakes, respectively. Figures 13 and 14 show the comparison of the bearing displacement between experimental and analytical results under various earthquakes. It is clearly

demonstrated from these simulated results that the proposed formulation can well simulate the response of a structure isolated with proposed isolators.

4. CONCLUSIONS

The base isolation technology is popular in the applications of updating the earthquake resistance capability of structures. The TFPS isolator proposed in this study is capable of having different radii in the upper and lower trench concave surfaces in the two orthogonal directions. By virtue of different natural frequencies in two directions, the isolator displacements in two directions can be optimized, especially for a structure possessing very different natural frequencies in two directions. Furthermore, the good efficiency in seismic mitigation had been proven through shaking table tests in this study. In addition, analytical results using proposed mathematical formulations can well predict the response of a structure isolated with TFPS isolators under seismic loadings.

REFERENCES

- [1] Tsai, C.S. (1996). Nonlinear Stress Analysis Techniques - NSAT. Department of Civil Engineering, Feng Chia University, Taichung, Chinese Taiwan.
- [2] Tsai, C.S., Chiang, T.C. and Chen, B.J. (2003). Seismic Behavior of MFPS Isolated Structure under Near-Fault Sources and Strong Ground Motions with Long Predominant Periods. *Seismic Engineering 2003, ASME*, Edited by J. C. Chen, Cleveland, Ohio, U.S.A., 73-79.
- [3] Tsai, C.S., Chiang, T.C. and Chen, B.J. (2005). Experimental evaluation of piecewise exact solution for predicting seismic responses of spherical sliding type isolated structures. *Earthquake Eng. Struct. Dyn.* **34**, 1027-1046.
- [4] Tsai, C.S., Chen, W.S., Chiang, T.C., and Chen, B.J. (2006). Component and shaking table tests for full scale multiple friction pendulum system. *Earthquake Eng. Struct. Dyn.* **35:13**, 1653-1675.
- [5] Fenz, D.M. and Constantinou, M.C. (2006), "Behaviour of the double concave Friction Pendulum bearing", *Earthquake Eng. Struct. Dyn.* **35:11**, 1403-1424.
- [6] Tsai, C.S., Lu, P.C. and Chen, W.S. (2006). Shaking Table Tests of A Building Isolated with Trench Friction Pendulum System. *Seismic Engineering 2006, ASME*, Edited by James F. Cory, Vancouver, BC, Canada, July 23-27, NO. PVP2006-ICPVT11-93253.
- [7] Tsai, C.S., Lin, Y.C. and Chen, W.S. (2006). Seismic behavior of high-tech facility isolated with a trench friction pendulum system. *Seismic Engineering 2006, ASME*, Edited by James F. Cory, Vancouver, BC, Canada, July 23-27, NO. PVP2006-ICPVT11-93474.

Table 1 Comparison of roof acceleration between the structure with and without TFPS isolator

Max. Response	PGA	Roof Acceleration (g)	
		EL Centro	Chi-Chi
Earthquake			
Fixed-Base Structure	0.25g	0.77g	0.43g
	0.38g	1.16g	0.64g
	0.50g	1.55g	0.85g
	0.63g	1.94g	1.07g
Structure with TFPS	0.25g	0.19g	0.16g
	0.38g	0.21g	0.18g
	0.50g	0.23g	0.18g
	0.63g	0.24g	0.21g
Response Reduction	0.25g	75.32%	62.79%
	0.38g	81.90%	71.88%
	0.50g	85.16%	78.82%
	0.63g	87.63%	80.37%

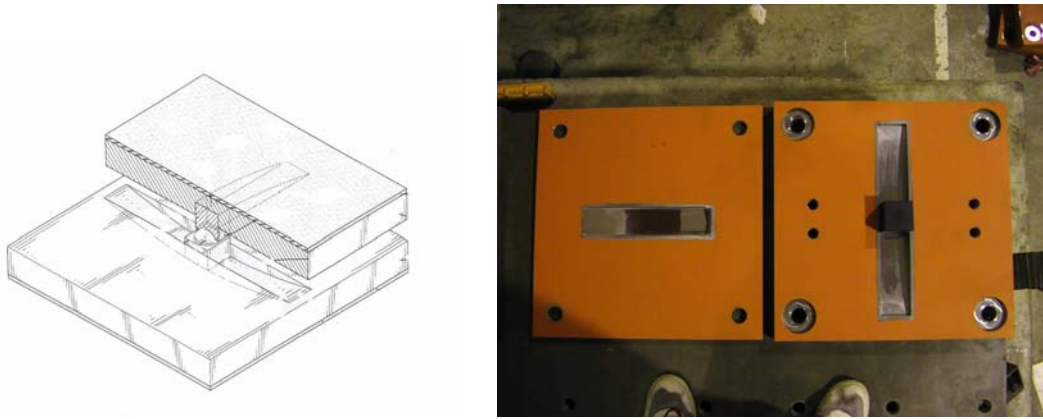


Figure 1 A perspective view and conformation of trench friction pendulum system

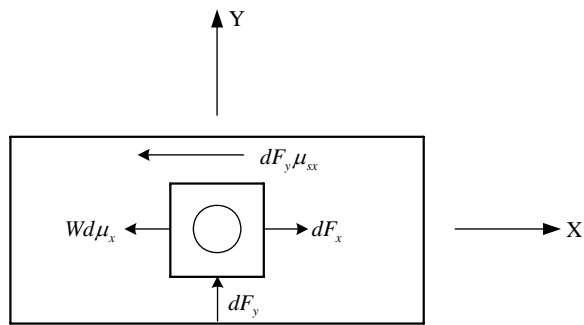


Figure 2 Top view of lower trench concave surface in X-direction

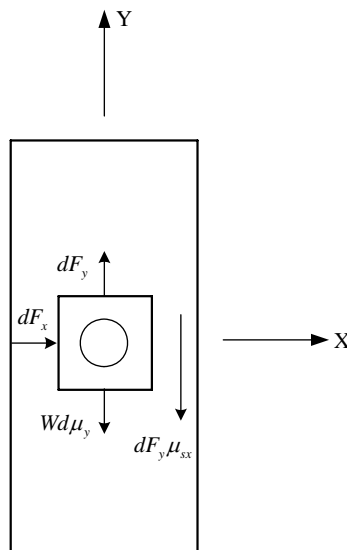


Figure 3 Top view of upper trench concave surface in Y-direction



Figure 4 TFPS Isolated structure on the shaking table

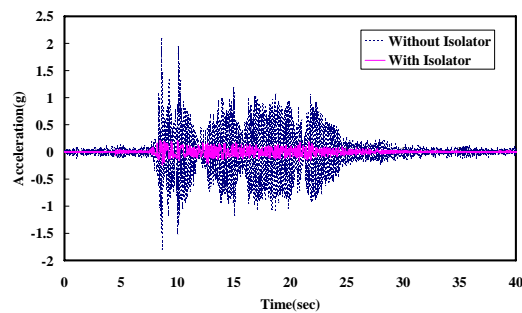


Figure 5 Roof acceleration of structure with and without TFPS isolators under El Centro earthquake of 0.63g in PGA

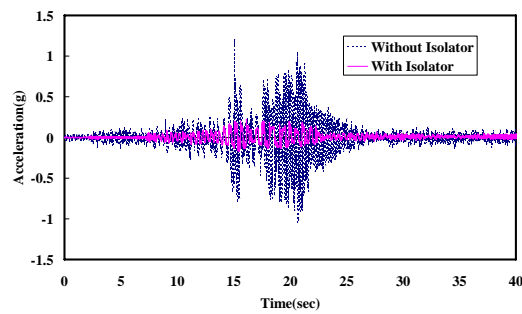


Figure 6 Roof acceleration of structure with and without TFPS isolators under Chi-Chi earthquake of 0.63g in PGA

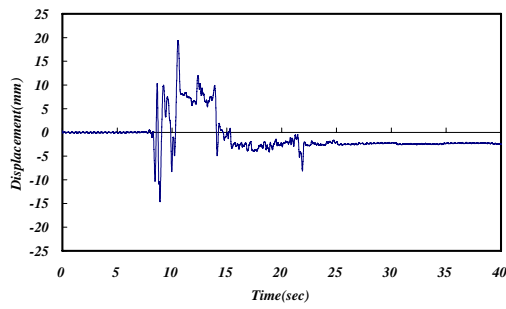


Figure 7 TFPS isolator displacement under El Centro of 0.63g in PGA

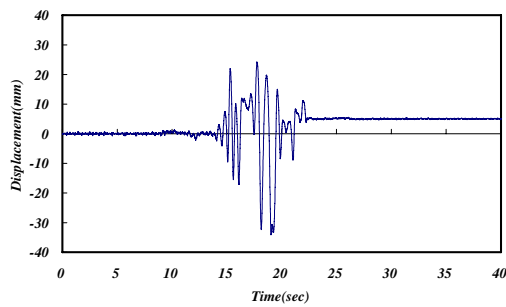


Figure 8 TFPS isolator displacement under Chi-Chi of 0.63g in PGA

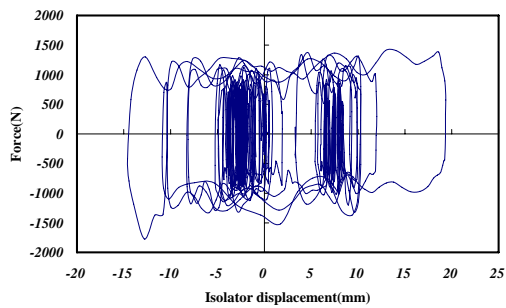


Figure 9 Hysteresis loops of TFPS isolator during El Centro earthquake of 0.63g in PGA

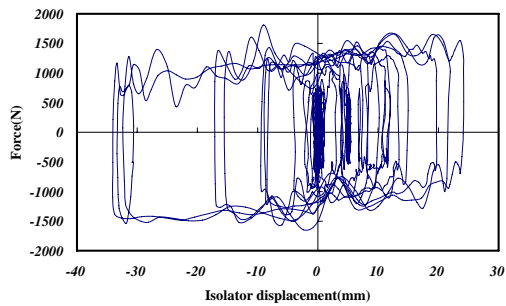


Figure 10 Hysteresis loops of TFPS isolator during Chi-Chi earthquake of 0.63g in PGA

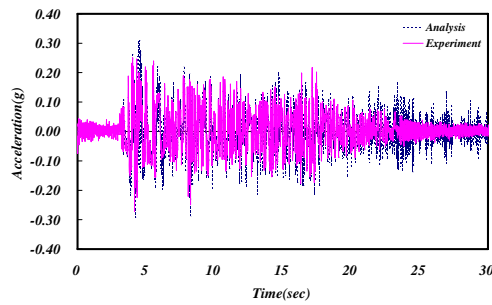


Figure 11 Comparison of roof acceleration of structure with TFPS isolators between experimental and numerical results under El Centro earthquake of 0.63g in PGA

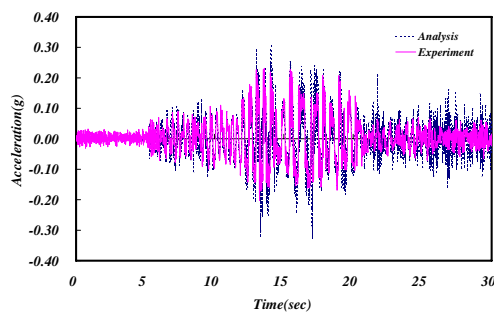


Figure 12 Comparison of roof acceleration of structure with TFPS isolators between experimental and numerical results under Chi-Chi earthquake of 0.63g in PGA

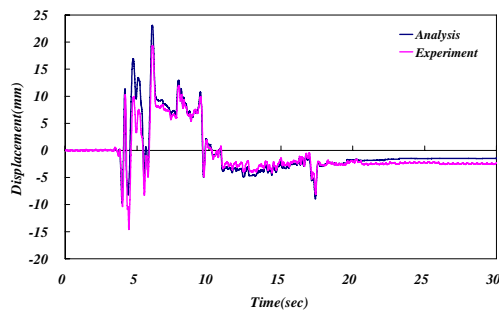


Figure 13 Comparison of bearing displacement of structure with TFPS isolators between experimental and numerical results under El Centro earthquake of 0.63g in PGA

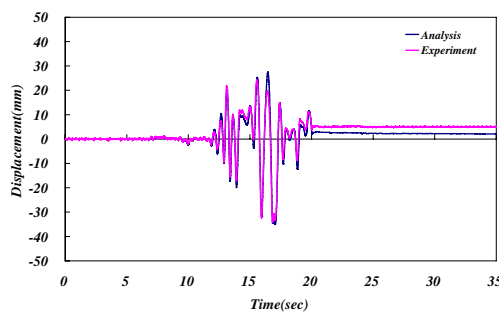


Figure 14 Comparison of bearing displacement of structure with TFPS isolators between experimental and numerical results under Chi-Chi earthquake of 0.63g in PGA